



*Original Article*

## Undrained lateral capacity of I-shaped concrete piles

Suraparb Keawsawasvong and Boonchai Ukritchon\*

*Geotechnical Research Unit, Department of Civil Engineering, Faculty of Engineering,  
Chulalongkorn University, Pathum Wan, Bangkok, 10330 Thailand*

Received: 18 May 2016; Revised: 1 September 2016; Accepted: 9 September 2016

---

### Abstract

This paper presents a new numerical solution for undrained lateral capacity of I-shaped concrete piles in accordance with the Thailand Industrial Standards. Two-dimensional finite element limit analysis with a plane strain condition in the direction of pile depth was employed to determine the stability of this problem. Six sections of I-piles were analyzed while parametric studies of each section were performed for a complete range of adhesion factors at the soil-pile interface, from smooth to rough piles, and two loading directions, where the I-pile was loaded normal to its major and minor axes. Failure mechanisms of the I-pile and its lateral capacity are discussed between different loading directions and compared with those of square piles. Design charts of all I-pile sections following Thailand Industrial Standards are proposed for an accurate and convenient prediction of undrained lateral capacity of I-shaped concrete piles in practice.

**Keywords:** pile, I-pile, limit analysis, numerical analysis, lateral capacity

---

### 1. Introduction

A driven pile is commonly used as a single pile or as part of a pile group to support various structures such as buildings, bridges, retaining walls, etc. In engineering practice, driven piles are generally prefabricated steel or reinforced concrete. Steel driven piles are either pipe piles or some form of beam section such as an H-pile. Concrete driven piles are available in square, octagonal, and built-in cross-sections, like I-piles. They are generally reinforced with prestressed tendons and may be precast for a required size and length specifically designed for a structure in certain soil conditions. One of the major advantages of driven concrete piles is that they make it possible to complete a construction project more quickly. In addition, they can be conveniently employed in places where it is not advisable to drill holes for bored piles during construction, for example at a site that has soft soil or high water pressure. Moreover, driven piles are much more favored for works in water such as wharf structures or jetties.

Analysis and design of the vertical capacity of piles can be commonly found in the literature (Bowles, 2001; Das, 2014; Federal Highway Administration [FHWA], 1998; Poulos & Davis, 1980). In addition to the vertical capacity of a pile, the lateral capacity is another major concern, since piles are generally subjected to lateral loadings that arise from earth pressure, wave forces in the sea, wind loading or forces caused by earthquakes (Reese Van & Impe, 2007). Therefore, the calculation for a pile's ultimate lateral load is important in order to evaluate its stability or safety factor against an applied lateral load in practice.

Like in many parts around the world, I-shaped concrete driven piles have become increasingly popular in Thailand for housing projects and retaining walls because of their cost-effectiveness and equivalent performance when compared to steel driven piles. In Thailand, prefabricated I-shaped concrete driven piles must meet the Thailand Industrial Standards (TIS 396-2549, 2007) that controls specifications (e.g. dimensions, concrete, reinforcement, etc.) and other quality requirements. Typical sections of I-shaped concrete piles following TIS 396-2549 (2007) are listed in Table 1. The ultimate vertical capacity of those piles can be calculated by a conventional static method; however, there

---

\* Corresponding author.

Email address: boonchai.uk@gmail.com

Table 1. Geometrical parameters of I-piles (after TIS 396-2549, 2007).

Section I-Bx B	Dimension (mm)					Area (mm <sup>2</sup> ) A
	B	K	L	O	U	
I-180x180	180	60	75	30	70	27,450
I-220x220	220	65	85	50	80	38,600
I-260x260	260	65	85	90	90	48,900
I-300x300	300	75	105	90	100	66,000
I-350x350	350	85	115	120	120	88,000
I-400x400	400	110	140	120	160	124,000
I-450x450	450	120	160	130	170	154,900

is no available solution for the lateral resistance of an I-pile. Thus, a simplification for an I-shaped section has to be made by approximating it to be a circular pile (Martin & Randolph, 2006; Randolph & Houlsby, 1984) or a rectangular pile (Keawsawasvong & Ukritchon, 2016; Ukritchon & Keawsawasvong, 2017) with which available solutions can be utilized. However, the validity of such simplification is questionable, and the accuracy of prediction cannot be assessed.

This paper considers a determination of undrained lateral capacity of I-shaped concrete piles in cohesive soils, where exact dimensions of I-shaped geometry of TIS 396-2549 (2007) in Table 1 are considered in the analysis. A general layout of the problem definition is shown in Figure 1. For the I-shaped concrete pile with an equal dimension of web and flange,  $B$  is embedded in a homogenous clay layer with constant undrained shear strength ( $s_u$ ). The clay obeys the rigid-perfectly plastic Tresca material with the associated flow rule.

In a real problem of laterally loaded piles, the ultimate lateral capacity of piles increases with depth from an initial low value at the ground surface to a maximum value at a certain depth, after which it remains constant throughout the deeper length of the pile. Thus, in this study, the pile is assumed to be very long, such that a lateral translation at depths located far from the ground surface essentially takes place under plane strain conditions. The limiting pressure at the deeper depth of the pile corresponds to the full-flow

failure mechanism around the pile (Murff & Hamilton, 1993). Because of the long pile assumption, the two-dimensional (2D) plane strain condition in the direction of pile depth is applicable. This paper aims to determine the ultimate lateral capacity of I-shaped concrete piles, where the full-flow failure mechanism develops.

The undrained lateral capacity of an I-shaped concrete pile is presented in terms of the dimensionless lateral load factor,  $N$  using the concept of dimensional analysis by Butterfield (2009) as:

$$N = \frac{P}{Bs_u} = f(\alpha) \quad (1)$$

where  $N$  is the undrained lateral capacity of pile per unit length,  $P$  is the lateral limit load of pile per unit length, and  $\alpha$  is the adhesion factor.

Adhesion factor ( $\alpha$ ) at the soil-pile interface is also considered in this study for the complete range from 0 (smooth) to 1 (rough) and defined as:

$$\alpha = s_{ui} / s_u \quad (2)$$

where  $s_{ui}$  is the undrained shear strength at soil-pile interface and  $s_u$  is the undrained shear strength of surrounding soil.

Laterally loaded piles were first studied by Broms (1964) based on the assumed slip line pattern. Ultimate lateral load per unit length, or ultimate lateral resistance, was proposed for several sections. The geometrical section of piles in Broms's works included circular piles, rotated square piles, and plate sections. Previous works of ultimate lateral load mostly focused on the circular section of piles. Randolph and Houlsby (1984) employed two-dimensional lower bound and upper bound plastic calculations based on the method of characteristics for circular piles in clay to derive an analytical closed-form solution for this problem. However, the exact lateral limit load of piles could only be found for rough piles while their upper and lower bound solutions were not accurate for other values of adhesion factor. Later, Martin and Randolph (2006) presented an improved upper bound solution, which enables accurate bracketing of the exact solutions of laterally loaded circular piles, when utilizing the lower bound solution of Randolph and Houlsby (1984). Ukritchon (1998) studied a numerical solution for the ultimate

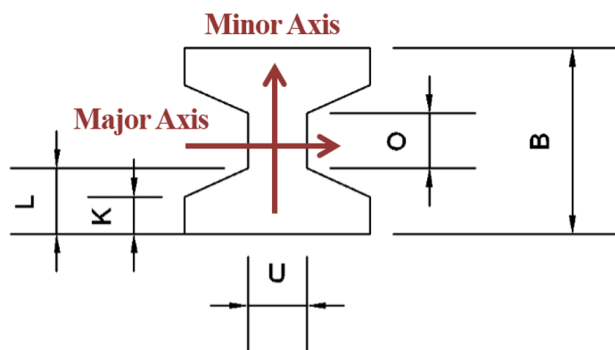


Figure 1. Problem geometry of an I-pile.

lateral load of a circular pile by finite element limit analysis that considered the effect of undrained strength anisotropy. Finite element limit analysis was also employed to solve the ultimate lateral load for problems encountered with two side-by-side circular piles with a symmetrical load (Georgiadis *et al.*, 2013a), a row of circular piles (Georgiadis *et al.*, 2013b), and two side-by-side circular piles with load inclination (Georgiadis *et al.*, 2013c).

At present, numerical tools are more advanced than those in the past. Thus, the finite element method has become popular in analyzing the ultimate load resistance of a pile. For example, Chaudry (1994), Klar (2008), and Zhang (2013) employed finite element analyses in calculations for piles under lateral load. However, their results were related to circular piles, while their applications are still questionable for a prediction of lateral capacity for I-shaped concrete piles under a full-flow failure mechanism. Even though various studies on the undrained lateral capacity of circular piles have been conducted in the past, there is no numerical solution of lateral limit load of I-shaped concrete piles available in the literature.

This paper presents a new plasticity solution for the undrained lateral capacity of I-shaped concrete piles in clay by finite element limit analyses (FELA). In this study, the dimensions of I-pile sections were based on Thailand Industrial Standards, TIS 396-2549 (2007), as shown in Table 1. Plasticity solutions of undrained lateral capacity of I-shaped piles are determined for a pile that is loaded either normal to its major or minor axes corresponding to the largest and smallest moments of inertia of their axes of symmetry. The adhesion factor,  $\alpha$  is studied in the complete range from 0 (smooth) – 1 (rough). Plasticity solutions of various sections of I-piles are compared with the solutions of square piles, while FELA solutions of circular piles are validated by existing solutions of Randolph and Houlsby (1984), and Martin and Randolph (2006). Failure mechanisms associated with each loading direction are discussed and postulated.

## 2. Numerical Methods

A commercial finite element limit analysis (FELA) software, OptumG2 (Krabbenhoft *et al.*, 2015), was employed to analyze the ultimate lateral load of I-piles in clay. This powerful numerical technique has been successfully applied to solve various stability problems in geotechnical engineering as demonstrated by Sloan (2013). The following summarizes aspects of numerical modeling of FELA in OptumG2, specifically related to the current study of a full-flow failure mechanism of I-shaped concrete piles. Full details of the numerical procedures in OptumG2 can be found in (Krabbenhoft *et al.*, 2015).

In finite element limit analysis, clay with constant undrained shear strength ( $s_u$ ) is modeled as a solid element with Tresca material and the associated flow rule. Because of the full-flow failure mechanism employing the plane strain condition in the direction of pile depth, clay is defined as a

weightless material with zero unit weight (i.e.,  $\gamma = 0$ ). Exact dimensions of an I-pile according to TIS 396-2549 (2007) in Table 1 are accurately modeled without any approximation. Six sections of an I-pile that range from the smallest size, 180×180 mm, to the largest size, 450×450 mm, are considered in the analysis. Each I-pile is modeled as the rigid solid element with a shear strength that is automatically defined by the software using a high value to ensure this behavior. The lateral load applied normally to either the major or minor axis of I-pile causes the full-flow failure mechanism around the pile. The major and minor axes of a pile correspond to the largest and smallest moments of inertia of their axes of symmetry. Numerical models of an I-pile loaded normally along these axes are illustrated in Figures 2(a) and 2(b), respectively. Interface elements between the clay and pile are used around the perimeter of I-pile. The adhesion factor at the soil-pile interface defined in equation (1) is studied in the range of 0 (smooth) – 1 (rough) with an increment of 0.25. For the full-flow failure mechanism, the study of Martin and White (2012) indicated that there was no difference in the solutions for modeling the soil-pile interface between the full tension and tension cut-off cases, which resulted in the same solution for undrained capacity of very deep pipelines in weightless soil. Thus, the soil-pile interfaces are modeled as the full tension case in this study. Owing to the symmetry of the I-pile geometry and loading, only half of the problem is considered as a numerical model. The external boundaries of the model are fixed in the normal direction of the planes while their tangential movements are free. Such boundary conditions satisfy the centerline of the models with both loading directions. The boundary size of the domain must be sufficiently large such that it the plastic shear zone does not intersect the external boundaries (except at the centerline of the problem) and is contained within the domain. Therefore, the upper and lower bound limit loads are not altered by an extension of the domain size, and there is no influence of the domain size on the computed solutions.

OptumG2 is used to perform a separate calculation of rigorous upper and lower bound limit analyses of a laterally loaded I-pile. Soil and I-shaped concrete piles are discretized into triangular elements in both analyses. For upper bound analysis, the best upper bound limit load is optimized by finding the minimum collapse load that satisfies a kinematically velocity field defined by the compatibility and associated flow rule equations at triangular elements and velocity discontinuities at soil-pile interfaces and velocity boundary conditions. For lower bound analysis, the best lower bound limit load is optimized by finding the maximum collapse load that satisfies a statically admissible stress field defined by the stress equilibrium equations at triangular elements and stress discontinuities of all shared edges of adjacent elements (including soil-pile interfaces), stress boundary conditions, and no stress violation of yield criterion. Both numerical upper and lower bound problems are formulated into a second-order conic programming (SOCP) (Krabbenhoft *et al.*, 2007) where the upper and lower bound loads are optimized

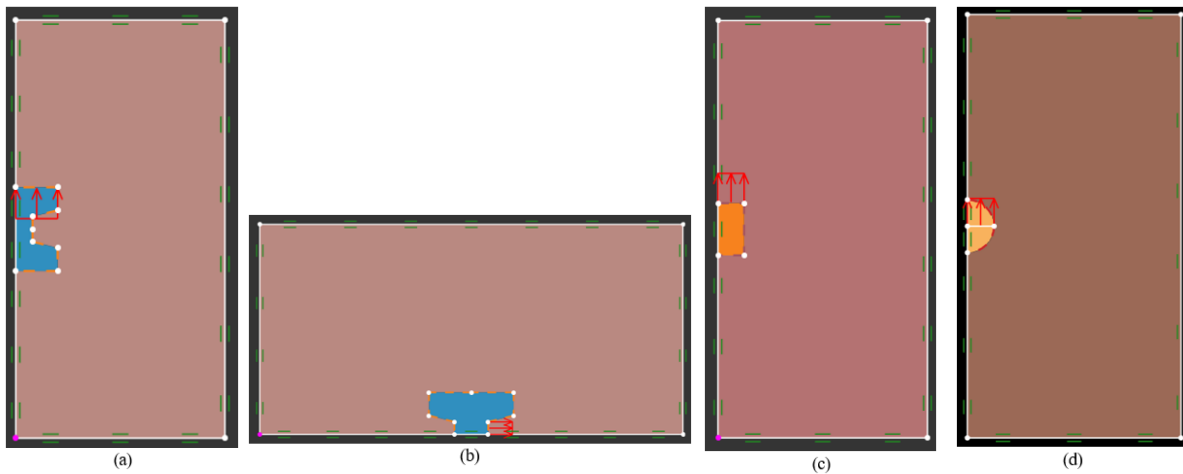


Figure 2. Numerical models in OptumG2: (a) I-pile loaded normal to the major axis, (b) I-pile loaded normal to the minor axis, (c) square pile, and (d) circular pile.

by an interior point optimizer (Krabbenhoft *et al.*, 2006) to obtain the minimum and maximum lateral limit load of I-piles, respectively.

In addition, mesh adaptivity (e.g., Lyamin *et al.*, 2005; Martin, 2011), a powerful feature in OptumG2, was employed in both the upper and lower bound analyses to determine the tight upper and lower bound solutions. In this study, the models of I-piles are analyzed by OptumG2 using the feature of mesh adaptivity starting at 5,000 elements and increasing to 10,000 elements in five adaptive iterations.

Note that analyses of two sections of circular and square piles are also performed as shown in Figures 2(c) and 2(d). The former is used for a validation with previous analytical solutions of undrained lateral capacity of circular piles, while the latter is used to compare with the lateral capacity of I-piles and to check if the lateral capacity of I-piles can be normalized to those of square piles.

### 3. Results and Discussion

Figure 3(a) shows a validation of undrained lateral capacity of circular piles,  $P/s_u B$  (i.e.,  $B$  = pile diameter) between FELA solutions and analytical upper and lower bound solutions by Randolph and Houlsby (1984), and Martin and Randolph (2006), respectively. Bound solutions of square piles are also shown in this plot. For circular and square piles with all adhesion factors, the exact lateral limit load of pile can be accurately bracketed by computed upper and lower bound solutions within 0.7% and 2.3%, respectively. Excellent agreement between the lateral capacity of circular piles of the present study and that of previous solutions could be observed. The lateral capacity of a circular pile is generally smaller than that of square pile by about 30-35%. Figures 3(b) and 3(c) show the incremental displacement vector predicted by FELA for circular piles with a smooth surface ( $\alpha = 0$ ) and rough surface ( $\alpha = 1$ ), respectively. It should be noted that predicted failure mechanisms of FELA

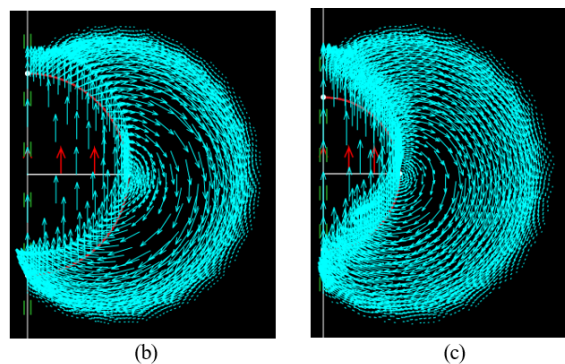
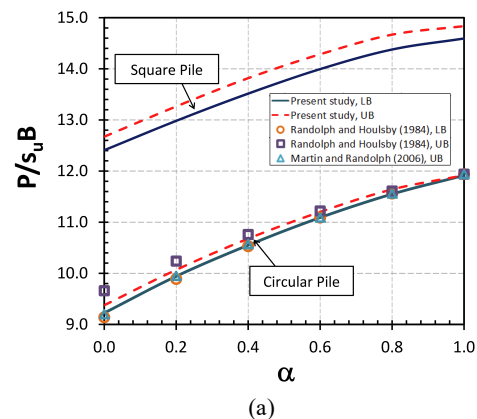


Figure 3. (a) Comparison of undrained lateral capacity of circular and square piles between the present study and previous solutions; Failure mechanism of circular piles: (b) smooth pile ( $\alpha = 0$ ) and (c) rough pile ( $\alpha = 1$ ).

correspond very well with the slip line solutions of Martin and Randolph (2006) for smooth and rough circular piles, where the results of the latter are omitted.

Figures 4(a) to 4(c) show the failure mode of rough square piles predicted by FELA. The failure mechanisms include the final adaptive mesh, Figure 4(a), vector of incre-

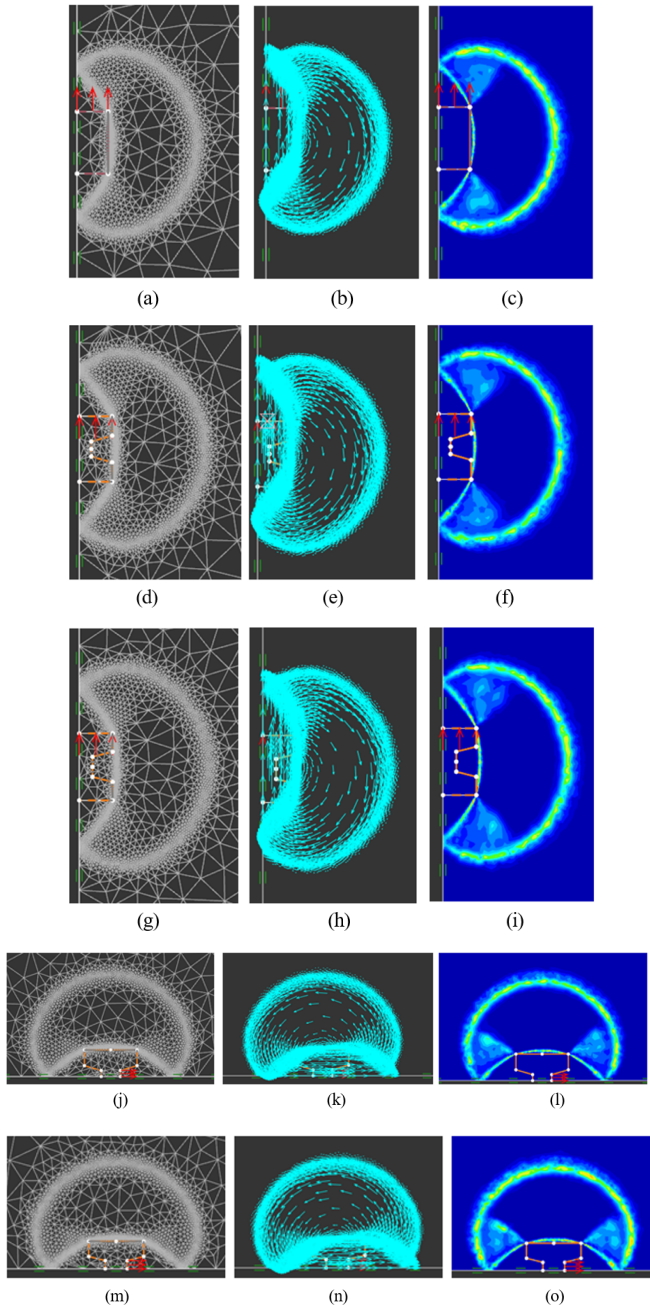


Figure 4. Failure mechanism of rough square piles: (a) Final adaptive mesh, (b) Incremental displacement vector, and (c) Incremental shear strain; Failure mechanism of rough I-pile section I-220×220 loaded normal to the major axis: (d) Final adaptive mesh, (e) Incremental displacement vector, and (f) Incremental shear strain; Failure mechanism of rough I-pile section I-400×400 loaded normal to the major axis: (g) Final adaptive mesh, (h) Incremental displacement vector, and (i) Incremental shear strain; Failure mechanism of rough I-pile section I-220×220 loaded normal to the minor axis: (j) Final adaptive mesh, (k) Incremental displacement vector, and (l) Incremental shear strain; Failure mechanisms of I-pile section I-400×400 loaded normal to the minor axis: (m) Final adaptive mesh, (n) Incremental displacement vector, and (o) Incremental shear strain.

mental displacement, Figure 4(b), and shear dissipation contour, Figure 4(c). It can be observed that the plastic flow of a square pile consists of two rigid triangular zones located on the front and back sides of the pile and radial shear zone on the sides of the pile starting from the front rigid triangular zone and ending at the back one. The radial shear zone joining corners of two triangular rigid zones appears like an ellipse. There is also a concentration elements found where there is a high degree of shearing around the edges of the square pile as well as inclined edges of the triangular zones and, perimeter of the radial and elliptical shear zones, which indicates the development of shear bands.

Figures 4(d) to 4(f) and 4(g) to 4(i) compare the failure mechanisms of rough I-piles with two sections I-220×220 and I-400×400 loaded normal to the major axis, respectively. Basically, the pattern of failure mechanism of I-220×220 is comparable to that of I-400×400, except that the latter has a larger plastic zone. Results of the rough I-pile sections I-220×220 and I-400×400 loaded normal to the minor axis are illustrated in Figures 4(j) to 4(l) and 4(m) to 4(o), respectively. In general, there are a number of similarities in failure mechanisms between I-piles loaded normal in both directions (i.e. major and minor axes) and square piles.

Figure 5 compares the failure mechanisms of square piles for three different adhesion factors. The failure mechanisms include the final adaptive mesh, Figures 5(a) to 5(c), the vector of incremental displacement, Figures 5(d) to 5(f), and the incremental shear strain contour, Figures 5(g) to 5(i). It can be observed that the size of radial shear zone depends on the adhesion factor, where a rough square pile produces a plastic zone that is larger than that of a smooth pile. In addition, the size of the rigid triangular zone in the front and back sides of square piles is affected by the adhesion factor. Lastly, the rigid zone that is adjacent to the side of pile is bigger and clearly seen in the case of rough piles. Figures 6(a) to 6(r) compare the failure mechanisms of I-pile section I-220×220 loaded normal to the major and minor axes. The influence of the adhesion factor on the predicted failure mechanism is presented in those figures. Note that results of I-pile section I-200×200 are similar to those of I-400×400, and thus the latter results are omitted. Apparently, the effects of adhesion on the failure mechanisms of I-piles loaded normal at both axes are similar to those of square piles, as described earlier. It can be observed that there are some differences in the predicted failure mechanism of a smooth I-pile between loading normal to the major and minor axes. For rough piles, there is no difference in the predicted failure mechanisms for the two loading directions.

Ultimate lateral load of an I-pile is represented as the dimensionless lateral capacity factor,  $N = P/s_u B$ , where  $P$  = ultimate load,  $s_u$  = undrained shear strength of clay and,  $B$  = size of I-pile. Design charts of the undrained lateral capacity of I-piles loaded normal to the major and minor axes are presented in Figures 7 and 8, respectively. For all cases, the difference between the upper and lower bound solutions of I-piles loaded normal to the major and the minor axes are

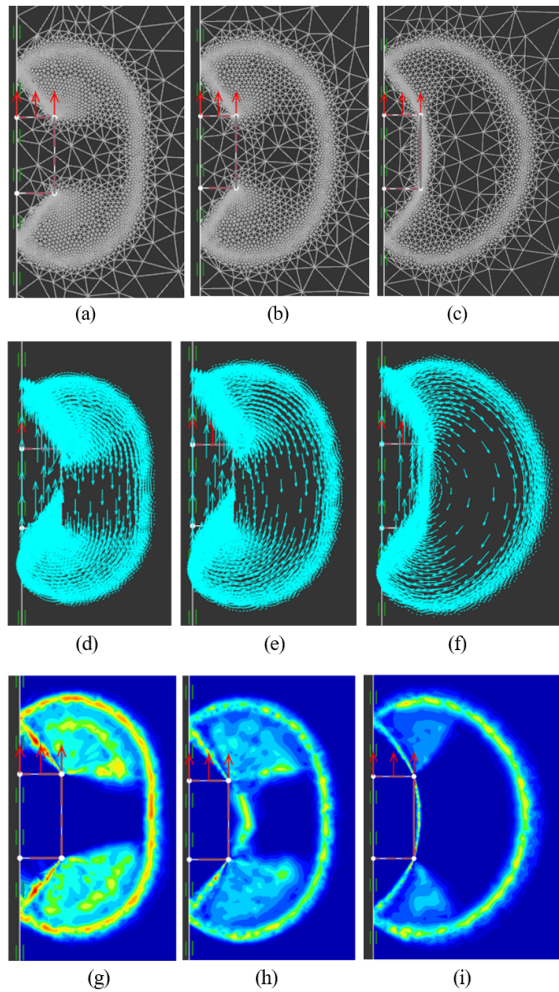


Figure 5. Final adaptive mesh of square piles: (a)  $\alpha = 0$ , (b)  $\alpha = 0.4$ , and (c)  $\alpha = 1$ , Incremental displacement vector of square piles: (d)  $\alpha = 0$ , (e)  $\alpha = 0.4$ , and (f)  $\alpha = 1$ , and Incremental shear strain of square piles: (g)  $\alpha = 0$ , (h)  $\alpha = 0.4$ , and (i)  $\alpha = 1$ .

within 4.3% to 2.4%, respectively. Figure 7 shows the relationship between the lateral capacity factor of an I-pile loaded normal to the minor axis and adhesion factor,  $\alpha$ . Since the computed plasticity solutions are accurate, the average solutions between the upper bound and lower bound solutions are used to plot the curve of each I-pile. Note that the curve of square piles is shown in this plot. Very clearly, the lateral capacity factors of I-piles loaded normal to the minor axis are practically identical to those of square piles for all values of adhesion factors. This result indicates that the soil plug within each flange of an I-pile behaves as a rigid body once it is loaded normal to its minor axis at the limit state.

Figure 8 shows the relationship between the lateral capacity factor of an I-pile loaded normal to the major axis and adhesion factor,  $\alpha$ . Like the results in Figure 7, the curve of each I-pile corresponds to the average of the upper bound and lower bound solutions. In this figure, each line corres-

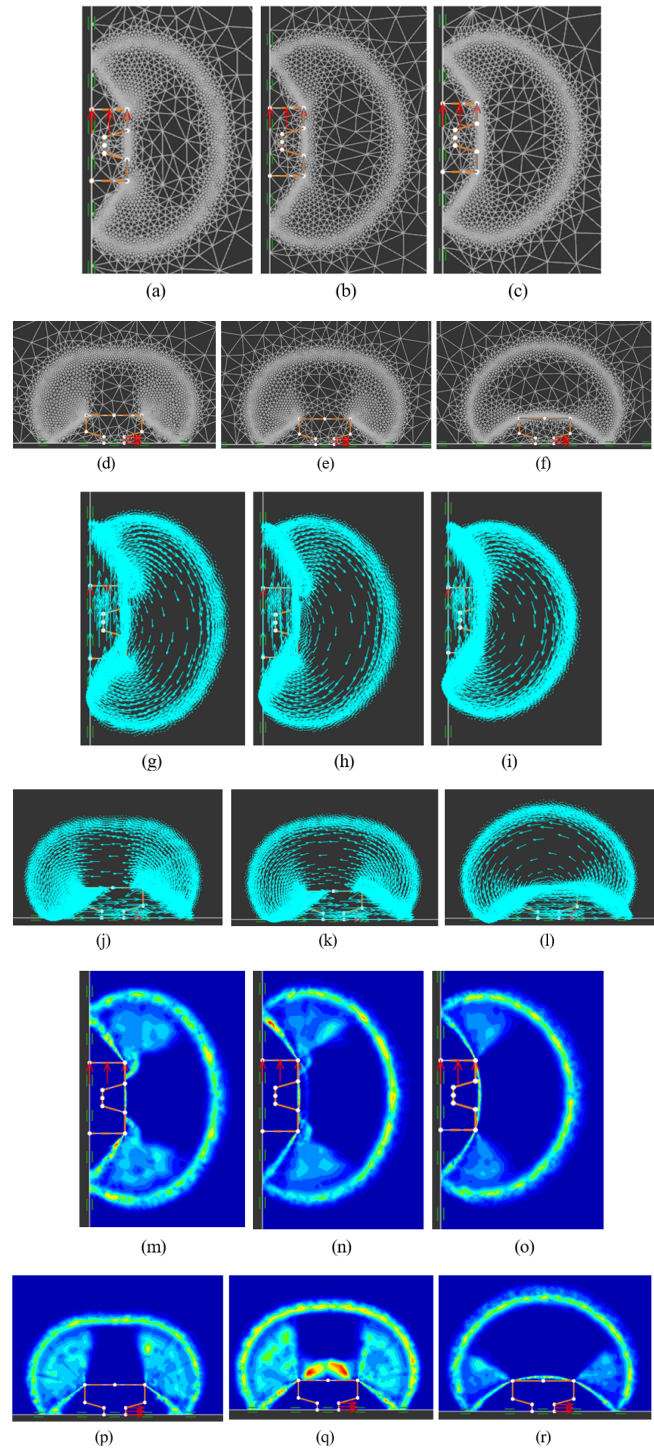


Figure 6. Final adaptive mesh of I-pile section I-220 $\times$ 220 loaded normal to the minor axis: (a)  $\alpha = 0$ , (b)  $\alpha = 0.4$ , and (c)  $\alpha = 1$ , and loaded normal to the major axis: (d)  $\alpha = 0$ , (e)  $\alpha = 0.4$ , and (f)  $\alpha = 1$ ; Incremental displacement vector of I-pile section I-220 $\times$ 220 loaded normal to the major axis: (g)  $\alpha = 0$ , (h)  $\alpha = 0.4$ , and (i)  $\alpha = 1$ , and loaded normal to the major axis: (j)  $\alpha = 0$ , (k)  $\alpha = 0.4$ , and (l)  $\alpha = 1$ ; Incremental shear strain of I-pile section I-220 $\times$ 220 loaded normal to the major axis: (m)  $\alpha = 0$ , (n)  $\alpha = 0.4$ , and (o)  $\alpha = 1$ , and loaded normal to the major axis: (p)  $\alpha = 0$ , (q)  $\alpha = 0.4$ , and (r)  $\alpha = 1$ .

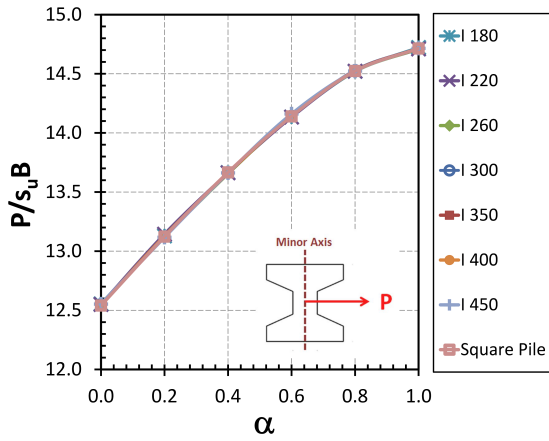


Figure 7. Relationship between undrained lateral capacity and adhesion factor of I-piles loaded normal to the minor axis.

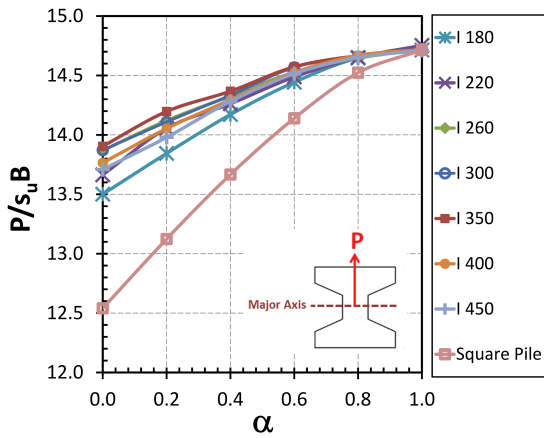


Figure 8. Relationship between undrained lateral capacity and adhesion factor of I-piles loaded normal to the major axis.

ponds to a different size I-pile loaded normal to the major axis, but the bottom line corresponds to the results of square piles. In general, expected trends of the curves are observed, where the lateral capacity factor of an I-pile increases with an increase of the adhesion factor. Note that for a smooth surface ( $\alpha = 0$ ), the lateral capacity of all sections of I-piles loaded normal to the major axis fall in the range of 13.5-13.9, which is higher than that of a square pile with the lateral capacity of 12.5. For an I-pile loaded normal to the major axis, the largest and smallest lateral capacities correspond to I-pile sections I-350x350 and I-180x180, respectively. Generally, the  $N$  value increases non-linearly with an increase of  $\alpha$ . When  $\alpha$  approaches 1 (rough pile), the  $N$  value for all sections of I-piles loaded normal to the major axis and that of square piles converges to a value of 14.7.

Figure 9 shows the ratio of undrained lateral capacity of an I-pile loaded normal to the major axis to that loaded normal to the minor axis,  $(P/s_u B)_{major} / (P/s_u B)_{minor}$ . It can be seen that for the same I-pile section, its lateral capacity of the major axis is larger than that of the minor axis by approximately 7-12%. A larger difference in lateral capacity between two loading directions can be seen for smooth piles, while

a smaller difference in lateral capacity among two loading directions becomes smaller once the adhesion factor of the I-pile is increased. This result implies that the soil plugs adjacent to each flange of an I-pile have some influence on the lateral pile capacity of the major axis provided that the adhesion factor is less than 1. Once the pile is fully rough ( $\alpha = 1$ ), there is no difference in lateral capacity of I-piles among different loading directions, which is practically identical to that of square piles.

#### 4. Conclusions

This paper studied the undrained lateral capacity of I-piles with sections that followed Thailand Industrial Standards (TIS 396-2549, 2007). A full-flow failure mechanism around a pile is assumed, and thus the plane strain condition is applied in the direction of pile depth. Two-dimensional plane strain finite element limit analysis was employed to determine the undrained lateral capacity of I-piles as well as circular and square piles. Two loading directions of I-piles were considered, including loading normal to the major and minor axes of pile. Due to the assumption of a full-flow failure mechanism, computed plasticity solutions are applicable for the piles in a deep zone that is not influenced by the ground surface. Six sections of I-piles, ranging from 180x180 mm to 450 x 450mm, were analyzed. For each section, a parametric study was carried out for a complete range of adhesion factor at the soil-pile interface for  $\alpha = 0$  (smooth)-1 (rough).

For all cases, the exact lateral limit load of circular piles, square piles, and I-piles can be accurately bracketed by computed upper and lower bound solutions within 0.7%, 2.3% and 4.3%, respectively. For all sections of piles, an influence of adhesion factor at the soil-pile interface on the lateral capacity of the piles is such that a higher lateral capacity of a pile is related to a higher adhesion factor. Predicted lateral capacity of circular piles can be validated very closely with previous solutions. It was found that the lateral capacity of square piles is generally larger than that of circular piles by about 30-35%. For an I-pile section, the lateral

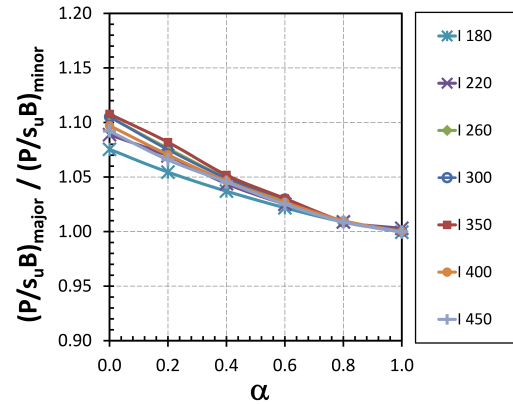


Figure 9. Ratio of undrained lateral capacity of I-piles loaded normal to the major axis to that loaded normal to the minor axis.

capacity of the minor axis is practically equal to that of a square pile of the same size and is generally smaller than that of the major axis by about 7-12%. A large difference in the lateral capacity of an I-pile between the major and the minor axes is observed for the case of a smooth I-pile. This result indicates that the lateral capacity of an I-pile loaded normal to the major axis is affected by the soil plug adjacent to the flange of the I-pile. However, this effect disappears when the I-pile is rough and the lateral capacity of both axes becomes equal to that of a square pile. Therefore, for a conservative design, the undrained lateral capacity of a square pile can be employed for a prediction of an I-pile with the same size axes for loading. For a more accurate design, the undrained lateral capacity of all I-pile sections following TIS 396-2549 (2007) can be conveniently and accurately predicted using proposed design charts when considering different loading directions.

## References

- Bowles, J. E. (2001). *Foundation analysis and design*. (5<sup>th</sup> ed.) New York, NY: McGraw-Hill.
- Broms, B. B. (1964). Lateral resistance of piles in cohesive soils. *Journal of the Soil Mechanics and Foundation*, 90(2), 27-63.
- Butterfield, R. (2009). Dimensional analysis for geotechnical engineering. *Géotechnique*, 49(2), 357-366. doi: 10.1680/geot.1999.49.3.357
- Chaudhry, A. R. (1994). *Static pile-soil-pile interaction in offshore pile groups* (Doctoral thesis, University of Oxford, Oxford, England).
- Das, B. M. (2014). *Principle of foundation engineering* (8<sup>th</sup> ed.) Boston, MA: Cengage Learning.
- Federal Highway Administration. (1998). *Design and construction of driven foundations* (Report No. FHWA-HI-97-013). Washington, DC: Author.
- Georgiadis, K., Sloan, S. W., & Lyamin, A. V. (2013a). Ultimate lateral pressure of two side-by-side piles in clay. *Géotechnique*, 63(9), 733-745. doi: 10.1680/geot.12.P030
- Georgiadis, K., Sloan, S. W., & Lyamin, A. V. (2013b). Undrained limiting lateral soil pressure on a row of piles. *Computers and Geotechnics*, 54, 175-184. doi: 10.1016/j.compgeo.2013.07.003
- Georgiadis, K., Sloan, S. W., & Lyamin, A. V. (2013c). Effect of loading direction on the ultimate lateral soil pressure of two piles in clay. *Géotechnique*, 63(13), 1170-1175. doi: 10.1680/geot.13.T.003
- Keawsawasvong, S., & Ukritchon, B. (2016). Ultimate lateral capacity of two dimensional plane strain rectangular pile in clay. *Geomechanics and Engineering*, 11(2), 235-251. doi: 10.12989/gae.2016.11.2.235
- Krabbenhoft, K., Lyamin, A. V., & Sloan, S. W. (2006). *SONIC: A conic programming code for plasticity problems: Version 1.0/LA: SOCP for limit analysis authors, illustrated edition*. New South Wales, Australia: Centre of Full Employment and Equity, University of Newcastle.
- Krabbenhoft, K., Lyamin, A. V., & Sloan, S. W. (2007). Formulation and solution of some plasticity problems as conic programs. *International Journal of Solids and Structure*, 44, 1533-1549. doi: 10.1016/j.ijsolstr.2006.06.036
- Klar, A., & Randolph, M. F. (2008). Upper-bound and load-displacement solution for laterally loaded piles in clays based on energy minimization. *Géotechnique*, 58(10), 815-820. doi: 10.1680/geot.2007.00197
- Krabbenhoft, K., Lyamin, A., & Krabbenhoft, J. (2015). Optum computational engineering (OptumG2). [Computer software]. Retrieved from <https://www.optumce.com>
- Lyamin, A., Sloan, S. W., Krabbenhoft, K., & Hjiat, M. (2005). Lower bound limit analysis with adaptive remeshing. *International Journal for Numerical Methods in Engineering*, 63, 1961-1974. doi: 10.1002/nme.1352
- Martin, C. M. (2011). The use of adaptive finite element limit analysis to reveal slip-line fields. *Geotechnique Letters*, 1, 23-29. doi: 10.1680/geolett.11.00018
- Martin, C. M., & Randolph, M. F. (2006). Upper-bound analysis of lateral pile capacity in cohesive soil. *Géotechnique*, 56(2), 141-145. doi: 10.1680/geot.2006.56.2.141
- Martin, C. M., & White, D. J. (2012). Limit analysis of the undrained bearing capacity of offshore pipelines. *Géotechnique*, 62(9), 847-863. doi: 10.1680/geot.12.OG016
- Muff, J. D., & Hamilton, J. M. (1993). P-Ultimate for undrained analysis of laterally loaded piles. *Journal of Geotechnical Engineering*, 119(1), 91-107. doi: 10.1061/(ASCE)0733-9410(1993)119:1(91)
- Poulos, H. G., & Davis, E. H. (1980). *Pile foundation analysis and design*. New York, NY: John Wiley and Sons.
- Randolph, M. F., & Houlsby, G. T. (1984). The limiting pressure on circular pile loaded laterally in cohesive soil. *Géotechnique*, 34(4), 613-623. doi: 10.1680/geot.1984.34.4.613
- Reese Van, L. C., & Impe, W. F. (2007). *Single piles and pile groups under lateral loading*. London, England: Taylor and Francis.
- Thai Industrial Standards Institute (2007). *Precast prestressed concrete piles-TIS 396-2549*. Bangkok, Thailand: Ministry of Industry.
- Ukritchon, B. (1998). *Application of numerical limit analyses for undrained stability problems in clay* (Doctoral thesis, Massachusetts Institute of Technology, Massachusetts).
- Ukritchon, B., & Keawsawasvong, S. (2017). Undrained lateral capacity of rectangular piles under a general loading direction and full flow mechanism. *KSCCE Journal of Civil Engineering*. doi: 10.1007/s12205-017-0062-7
- Zhang, L. (2013). Nonlinear analysis of laterally loaded rigid piles in cohesive soil. *International Journal for Numerical and Analytical Method in Geomechanics*, 37, 201-220. doi: 10.1016/j.compgeo.2008.12.001